American Mineralogist, Volume 92, pages 91–97, 2007

Synchrotron powder X-ray diffraction study of the structure and dehydration behavior of sepiolite

Jeffrey E. Post,[1,*] David L. Bish,[2] and Peter J. Heaney[3]

[1]Department of Mineral Sciences, Smithsonian Institution, Washington, D.C. 20560-0119, U.S.A.
[2]Department of Geological Sciences, Indiana University, Bloomington, Indiana 47405-1405, U.S.A.
[3]Department of Geosciences, Pennsylvania State University, University Park, Pennsylvania 16802, U.S.A.

Abstract

Rietveld refinements using synchrotron powder X-ray diffraction data were used to study the crystal structure and dehydration behavior of sepiolite from Durango, Mexico. The room-temperature (RT) sepiolite structure in air compares well with previous models but reveals an additional zeolitic H_2O site. The RT structure under vacuum retained only ~1/8 of the zeolitic H_2O and the volume decreased by 1.3%. Real-time, temperature-resolved synchrotron powder X-ray diffraction data and Rietveld refinements were used to investigate the behavior of the sepiolite structure from 300 to 925 K. Rietveld refinements revealed that most of the zeolitic H_2O is lost by ~390 K, accompanied by a decrease in the *a* and *c* unit-cell parameters. Above ~600 K the sepiolite structure folds as one-half of the crystallographically bound H_2O is lost. Rietveld refinements of the "anhydrous" sepiolite structure reveal that, in general, unit-cell parameters *a* and *b* and volume steadily decrease with increasing temperature; there is an obvious change in slope at ~820 K suggesting a phase transformation coinciding with the loss of the remaining bound H_2O molecule.

Keywords: Sepiolite, Rietveld, synchrotron, powder diffraction

Introduction

Sepiolite is a hydrous Mg-rich silicate clay mineral with fibrous morphology that typically occurs as fine-grained, poorly crystalline masses. It occurs in a wide variety of geological environments and has been mined for centuries because of its many useful properties. Sepiolite boasts more than 100 commercial uses today in the pharmaceutical, fertilizer, and pesticide industries (Van Scoyoc et al. 1979; Jones and Galan 1988), and its versatile functionality derives from the large surface area and microporosity that are characteristic of the material. In recent years, sepiolite has received considerable attention with regard to the adsorption of organics, for use as a support for catalysts (Jones and Galan 1988), as a molecular sieve (Ruiz-Hitzky 2001), and as an inorganic membrane for ultrafiltration (Wang et al. 2001).

Sepiolite has a layer structure constructed of ribbons of 2:1 phyllosilicate modules that are linked triple silicate chains that sandwich Mg-(O,OH) octahedral strips (Fig. 1). The ribbons are linked by inversion of the SiO_4 tetrahedra through Si-O-Si bonds. Sepiolite has continuous tetrahedral sheets, but with tetrahedral apices pointing in opposite directions in adjacent ribbons. Unlike other phyllosilicates, it lacks continuous octahedral sheets. The structure has large tunnels parallel to the phyllosilicate ribbons that are partially occupied by H_2O molecules. The tunnels measure 3.7×10.6 Å in cross section.

The sepiolite structure was first deduced by Brauner and Preisinger (1956) from fiber X-ray diffraction patterns, and their model is orthorhombic with space group *Pnan*. Rautureau and Tchoubar (1976) calculated projected electron-density maps using electron-diffraction intensities that confirmed the model of Brauner and Preisinger (1956) but suggested the possibility of a split site for one of the Mg atoms and crystallographically bound H_2O molecules. Because of its fine-grained and poorly crystalline nature, it has not been possible to study the crystal structure of sepiolite using single-crystal diffraction methods, and consequently many details of the structure are still not well known. In this study, we used synchrotron powder X-ray diffraction data and Rietveld refinements to better characterize the structure and behavior of sepiolite. We refined room-temperature structures for both a fully hydrated sepiolite and one for which the zeolitic H_2O molecules were removed under vacuum.

In the second part of our study, we used temperature-resolved real-time synchrotron X-ray powder diffraction and Rietveld refinements to investigate in unprecedented detail changes in the sepiolite structure as it dehydrated from room temperature (RT) to 925 K. The Brauner and Preisinger (1956) structure model includes three types of H_2O: zeolitic H_2O molecules in the tunnels, crystallographically bound H_2O molecules that complete the coordination of the Mg atoms at the edges of the octahedral strips, and hydroxyl (OH) groups bonded to some of the Mg atoms. Numerous previous studies have monitored the dehydration of sepiolite using thermogravimetric analysis (TGA) and differential thermal analysis (DTA) methods (e.g., Preisinger 1959; Hayashi 1969; Nagata et al. 1974; Serna et al. 1975; Lokanatha et al. 1985; Ruiz et al. 1996; Weir et al. 2002).

* E-mail: postj@si.edu

0003-004X/07/0001–91$05.00/DOI: 10.2138/am.2007.2134

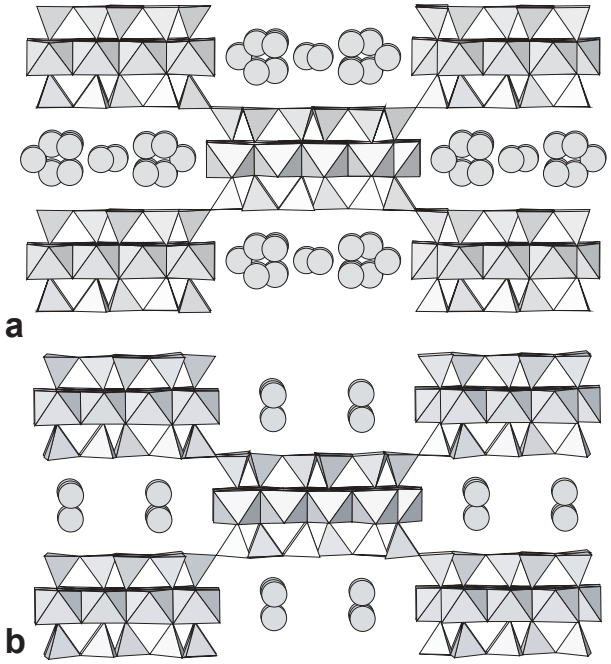

FIGURE 1. Polyhedral crystal structure representations, viewed along *c*, resulting from the Rietveld refinements for sepiolite (RT): (**a**) in air and (**b**) under vacuum. Shaded circles represent zeolitic H_2O molecules.

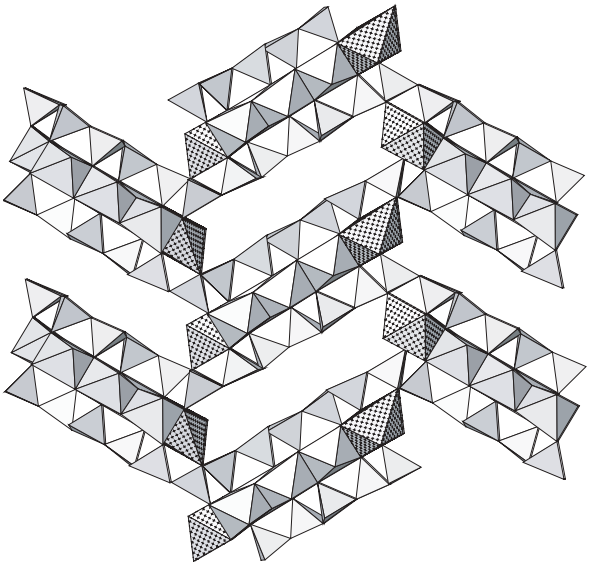

FIGURE 2. Folded structure resulting from the Rietveld refinement for sepiol-2H_2O (742 K) viewed along the monoclinic *c* axis. The dotted polyhedra at the edges of the octahedral strips represent the Mg4 coordination.

There is a general concurrence among these researchers that zeolitic H_2O is lost during heating from RT to ~415 K, or at RT under vacuum; bound H_2O molecules are released in two stages between ~525 and 875 K; and hydroxyl groups are lost above ~1075 K. Preisinger (1959, 1963) proposed that loss of the bound H_2O causes a phase change during which the structure folds by rotation of the phyllosilicate ribbons about an axis through the Si-O-Si corner bonds that link the ribbons (Fig. 2). Rautureau and Mifsud (1977) show high-resolution transmission electron microscope images that appear to confirm the existence of a folded "anhydrous" structure. Furthermore, the TGA results and an X-ray diffraction study by Nagata et al. (1974) suggest that there are two distinct "anhydrous" sepiolite phases, corresponding to the loss of the first and second bound H_2O molecules, respectively. We present here the results of a series of refinements of the "anhydrous" sepiolite structure over the temperature range ~666 to 925 °C that further confirm both the basic Preisinger (1959) folded-structure model and the existence of two "anhydrous" phases.

DATA COLLECTION AND REFINEMENT

The sepiolite sample used for this study (NMNH no. 92158-1) is from Durango, Mexico, and powder X-ray data revealed that it is exceptionally well ordered for sepiolite and free of impurity phases. Electron microprobe analyses (JEOL JXA-8900R) using samples embedded in epoxy, polished and carbon-coated yielded a result that is similar to the ideal chemical formula: $Mg_{16}Si_{24}O_{60}(OH)_8 \cdot nH_2O$. Because of the difficulty of analyzing fibrous, embedded samples, it was not possible to obtain water by difference. Thermogravimetric analysis on 11.8 mg of sample (Universal 3.3B TA Instruments), heating at 5 K/min to 1273 K yielded a total weight loss of ~18%, which is similar to results from previous studies (e.g., Preisinger 1959; Nagata et al. 1974). The sample used for X-ray diffraction was hand ground under acetone in an agate mortar and passed through a 400-mesh sieve. For the synchrotron X-ray diffraction (XRD) studies, samples were loaded into 0.7 and 0.5 mm quartz-glass capillaries for the RT and heating experiments, respectively. X-ray diffraction data were collected at beam line X7B of the National Synchrotron Light Source (NSLS), Brookhaven National Laboratory (BNL), using wavelengths of 0.9492 (RT samples in air and vacuum) and 0.9274 Å (heating experiment) and a MAR345 full imaging plate detector. Diffraction data used for the sepiolite structure refinements were collected at room temperature (300 K) from a sample in air and from a second sample under vacuum (1×10^{-6} torr).

The heating experiment was performed in air using a Blake Instruments furnace with a Pt-13%Rh coiled wire yoke encased in ZrO_2 cement (Brown et al. 1973). The temperature was varied with an Omega controller and monitored with a Chromel-Alumel thermocouple located ~2 mm from the specimen. The actual sample temperature was determined for the range 298 to 1273 K by a variety of phase and melting transitions and by the placement of an additional thermocouple in the sample position. The highly linear relationship between the observed and actual temperatures ($r^2 = 0.983$) allowed us to calculate a calibration curve with an estimated error of ±5 K for a given temperature. Temperature-resolved data from 300 to 925 K were collected as a series of 90 s exposures with a MAR345 full imaging plate detector. The temperature was increased continuously at 5.4 K/min and measurements were obtained every ~15 K, owing to down time for repositioning of the sample and reading the imaging plate; thus, each exposure encompassed a temperature range of ~8.1 K. During each exposure the sample was rotated through a 90° angle. Preferred orientation of the powder was eliminated through a combination of the specimen rotation, use of a capillary sample holder, and full intensity integration of the diffraction rings, as obtained using the program Fit2D (Hammersley et al. 1996) with a polarization factor of 0.93.

Rietveld refinements were performed using the General Structure Analysis System (GSAS) of Larson and Von Dreele (2001) using data measured over a range of temperatures from RT (in air and vacuum) to the point at which most of the bound H_2O was lost (925 K). The starting structural parameters for the sepiolite phyllosilicate modules were taken from Brauner and Preisinger (1956). The model for the "anhydrous" sepiolite was derived graphically from that illustrated by Preisinger (1959, 1963), and Mg-O and Si-O bond distances were optimized in a monoclinic unit cell ($P2_1/n$) using the GSAS bond distance constraint feature with a large weighting factor (F = 5000). Initially, the Si-O distances were constrained to 1.60 Å and the Mg-O distances to 2.03 Å. The diffraction pattern backgrounds were fit using a linear interpolation function. Peak profiles were modeled by a pseudo-Voigt profile function as parameterized by Thompson et al. (1987) with asymmetry corrections by Finger et al. (1994) and microstrain anisotropic broadening terms by Stephens (1999). Displacement parameters for a given atom type were constrained to be equivalent.

TABLE 1. Final Rietveld refinement parameters for sepiolite in air and under vacuum

	Air	Vacuum
Space group	*Pncn*	*Pncn*
Unit cell		
a (Å)	13.405(1)	13.248(1)
b (Å)	27.016(1)	27.053(1)
c (Å)	5.2750(1)	5.2616(2)
V (Å^3)	1910.4(1)	1885.7(2)
Refinement		
No. of data points	1871	2185
No. of reflections	1058	750
Diffraction range (d Å)	0.986–9.1	1.13–8.9
No. of variables	82	85
R (*F*^{2})	0.055	0.052
R_{wp}	0.021	0.020
χ^2	0.125	4.91

TABLE 2. Final Rietveld refinement parameters for sepiol-2H_2O (742 K) and anhydrous sepiolite (925 K)

	742 K	925 K
Space group	$P2_1/n$	$P2_1/n$
Unit cell		
a (Å)	23.446(4)	23.415(3)
b (Å)	11.352(3)	11.157(2)
c (Å)	5.2782(4)	5.2816(5)
β (°)	89.06(1)	89.21(1)
V (Å^3)	1407.7(5)	1379.7(5)
Refinement		
No. of data points	2023	2023
No. of reflections	1103	1065
Diffraction range (d Å)	1.13–6.6	1.13–6.6
No. of variables	121	121
R (*F*^{2})	0.010	0.013
R_{wp}	0.006	0.007
χ^2	0.48	0.54

During the initial cycles of refinement, only the background, scale, peak profile, and unit-cell parameters were allowed to vary. After convergence, difference-Fourier maps were calculated to locate the O atoms of the H_2O molecules in the tunnels (for the sample in air). These O atoms were added to the structure model and all atom positions and displacement parameters and occupancy factors of the O atoms of the H_2O molecules were refined. Soft constraints were used to limit the Si-O bond distances to within the range observed in similar silicate structures, e.g., tuperssuatsiaite (1.58–1.63 Å, <1.61 Å>; Cámara et al. 2002) and raite (1.59–1.65 Å <1.62 Å>; Pluth et al. 1997). The weighting factors for the constraints were gradually reduced. Attempts to eliminate the weighting factors completely for sepiolite resulted in Si-O distances of 1.55 (Si1-O1) and 1.68 Å (Si2-O6), and therefore the smallest weighting factor (F = 0.5) that yielded reasonable Si-O distances (i.e., 1.60–1.64 Å) was retained. The bond constraint χ^2 contribution accounted for 24.2 out of a total X^2 contribution of 224. For "anhydrous" sepiolite, the Si-O and Mg-O distances, except for those between Mg4 and O10, were constrained throughout the refinement (F = 50).

The final refinement parameters for RT sepiolite in air and vacuum are listed in Table 1, and results for "anhydrous" sepiolite (742 K) and anhydrous sepiolite (925 K) are included in Table 2. The refined atom positions for the samples in air and under vacuum at RT are not significantly different except for the zeolitic H_2O; therefore, the complete set of atom positions is given in Table 3 for the sample in air, and only those for the remaining zeolitic H_2O molecule are included for the sample under vacuum (The full set of atom positions for sepiolite under vacuum are listed in Appendix 1.)[1] Refined framework atom positions for "anhydrous" sepiolite were similar at all temperatures and therefore only the values determined at 742 K are reported in Table 4. Selected bond distances for RT sepiolite in air and "anhydrous" sepiolite (742 K) are reported in Tables 5 and 6, respectively. The final observed, calculated, and difference patterns for the RT sepiolite sample in air and "anhydrous" sepiolite (742 K) are plotted in Figures 3 and 4, respectively. As is often the case, the standard deviations calculated by GSAS for the unit-cell parameters are likely lower than the true errors (Post and Bish 1989). We present the errors calculated by GSAS in the tables of this paper with the understanding that the actual errors may be more than an order of magnitude greater than the calculated deviations.

TABLE 3. Atomic coordinates and isotropic displacement parameters for RT sepiolite (air) and for the zeolitic H_2O site (vacuum)

Atom	*x*	*y*	*z*	Site occupancy factor	U_{iso} (Å^2)*
Mg1	0	0.0297(7)	0.25	1.0	0.040(2)
Mg2	0	0.0850(7)	0.75	1.0	0.040(2)
Mg3	0	0.1434(5)	0.25	1.0	0.040(2)
Mg4	0	0.2049(4)	0.75	1.0	0.040(2)
Si1	0.2026(6)	0.0282(4)	0.586(2)	1.0	0.040(1)
Si2	0.1973(8)	0.1409(3)	0.576(2)	1.0	0.040(1)
Si3	0.2042(7)	0.1949(2)	0.070(2)	1.0	0.040(1)
O1	0.0824(7)	0.0276(7)	0.585(2)	1.0	0.035(1)
O2	0.0805(9)	0.0854(6)	0.081(2)	1.0	0.035(1)
O3	0.0762(8)	0.1431(5)	0.597(2)	1.0	0.035(1)
O4	0.0847(8)	0.1971(6)	0.077(2)	1.0	0.035(1)
O5	0.248(1)	0.0040(7)	0.324(2)	1.0	0.035(1)
O6	0.2451(9)	0.0849(4)	0.579(3)	1.0	0.035(1)
O7	0.243(1)	0.1708(7)	0.334(2)	1.0	0.035(1)
O8	0.249(1)	0.1736(7)	0.802(2)	1.0	0.035(1)
O9	0.25	0.25	0.089(6)	1.0	0.035(1)
O10 (H_2O)	0.088(1)	0.2596(5)	0.594(3)	1.0	0.035(1)
O11 (H_2O)	0.562(1)	–0.090(1)	–0.012(4)	0.91(2)	0.10
O12 (H_2O)	0.50	0.180(1)	0.25	1.0(3)	0.10
O13 (H_2O)	0.50	0.023(3)	0.25	0.43(3)	0.10
O14 (H_2O)	0.439(3)	0.157(3)	0.74(2)	0.33(3)	0.10
Vacuum					
O11 (H_2O)	0.562(6)	0.109(3)	0.50(1)	0.24(2)	0.10

* Isotropic displacement parameters for same atom types were constrained to be equal, and for 011–014 were set equal to 0.10.

TABLE 4. Atomic coordinates and isotropic displacement parameters for Sepiol-2H_2O (742 K)

Atom	*x*	*y*	*z*	Site occupancy factor	U_{iso} (Å^2)*
Mg1	0.0238(5)	0.023(1)	0.244(2)	1.0	0.02
Mg2	0.0862(6)	0.115(1)	0.729(2)	1.0	0.02
Mg3	0.1431(6)	0.179(1)	0.244(2)	1.0	0.02
Mg4	0.1942(5)	0.246(1)	0.719(2)	1.0	0.02
Si1	0.0869(6)	0.833(1)	0.561(2)	1.0	0.02
Si2	0.2012(5)	0.970(1)	0.539(2)	1.0	0.02
Si3	0.2504(6)	0.027(1)	0.028(2)	1.0	0.02
O1	0.0558(5)	0.959(1)	0.580(2)	1.0	0.025
O2	0.1024(5)	0.042(1)	0.074(2)	1.0	0.025
O3	0.1664(7)	0.0903(1)	0.568(3)	1.0	0.025
O4	0.2185(7)	0.153(2)	0.040(3)	1.0	0.025
O5	0.0680(9)	0.744(2)	0.340(3)	1.0	0.025
O6	0.1529(7)	0.870(2)	0.574(4)	1.0	0.025
O7	0.235(1)	0.950(2)	0.273(3)	1.0	0.025
O8	0.2387(9)	0.947(2)	0.784(3)	1.0	0.025
O9	0.3172(7)	0.034(2)	0.061(4)	1.0	0.025
O10 (H_2O)	0.2733(9)	0.211(3)	0.512(3)	1.0(2)	0.025
Si1b	0.9668(5)	0.234(1)	0.916(2)	1.0	0.02
Si2b	0.0807(5)	0.374(1)	0.894(2)	1.0	0.02
Si3b	0.1278(6)	0.454(1)	0.405(2)	1.0	0.02
O1b	0.0092(6)	0.124(1)	0.923(3)	1.0	0.02
O2b	0.0601(6)	0.174(2)	0.386(2)	1.0	0.025
O3b	0.1172(6)	0.257(1)	0.917(2)	1.0	0.025
O4b	0.1653(9)	0.336(1)	0.407(3)	1.0	0.025
O5b	0.9260(9)	0.227(2)	0.166(3)	1.0	0.025
O6b	0.0152(8)	0.332(2)	0.868(4)	1.0	0.025
O7b	0.092(1)	0.446(2)	0.152(3)	1.0	0.025
O8b	0.0798(8)	0.443(2)	0.627(3)	1.0	0.025

* Isotropic displacement parameters were fixed to typical values for silicate structures.

[1] Deposit Item AM-07-001, Appendix 1, the full set of atom positions for sepiolite under vacuum. Deposit items are available two ways: For paper copy contact the Business Office of the Mineralogical Society of America (see inside cover of recent issue) for price information. For an electronic copy visit the MSA web site at http://www.minsocam.org, go to the American Mineralogist Contents, find the table of contents for the specific volume/issue wanted, and then click on the deposit link there.

TABLE 5. Selected bond distances (Å) for sepiolite in air at RT

Mg1-O1	2.09(1) × 2	Mg2-O1	2.09(1) × 2
Mg1-O1	2.09(1) × 2	Mg2-O2	2.05(1) × 2
Mg1-O2	2.06 (1) × 2	Mg2-O3	2.04(1) × 2
<Mg1-O>	2.08	<Mg2-O>	2.06
Mg3-O2	2.10(1) × 2	Mg4-O3	2.12(1) × 2
Mg3-O3	2.10(1) × 2	Mg4-O4	2.08(1) × 2
Mg3-O4	2.06(1) × 2	Mg4-O10	2.06(1) × 2
<Mg3-O>	2.09	<Mg4-O>	2.09
Si1-O1	1.611(6)	Si2-O3	1.627(6)
Si1-O5	1.642(6)	Si2-O6	1.643(6)
Si1-O5	1.644(6)	Si2-O7	1.631(6)
Si1-O6	1.635(6)	Si2-O8	1.639(6)
<Si1-O>	1.63	<Si2-O>	1.64
Si3-O4	1.604(6)	O10-O8	3.13(2)
Si3-O7	1.627(7)	O10-010	2.93(3)
Si3-O8	1.639(7)	O10-O12	2.72(2)
Si3-O9	1.614(6)	O10-O14	2.47(8)
<Si3-O>	1.62	O12-O14	2.78(8)
O11-O11	3.01(4)	O12-O14	2.88(8)
O11-O12	2.87(3)	O13-O13	2.91(6)
O11-O13	2.35(6)	O14-O8	2.64(7)
O11-O14	2.32(8)		
O11-O14	2.79(8)		
O11-O14	2.79(8)		

Note: Soft constraints were applied to Si-O distances (see text) during refinement.

TABLE 6. Selected bond distances (Å) for sepiol-2H_2O (742 K)

Mg1-O1	2.07(1)	Mg2-O1	2.07(1)
Mg1-O1	2.08(1)	Mg2-O2	2.04(1)
Mg1-O2	2.05(1)	Mg2-O3	2.07(1)
Mg1-O1b	2.08(1)	Mg2-O1b	2.07(1)
Mg1-O1b	2.05(1)	Mg2-O2b	2.04(1)
Mg1-O2b	2.06(1)	Mg2-O3b	2.03(1)
<Mg1-O>	2.07	<Mg2-O>	2.05
Mg3-O2	2.04(1)	Mg4-O3	2.05(1)
Mg3-O3	2.07(1)	Mg4-O4	2.09(1)
Mg3-O4	2.08(1)	Mg4-O8	2.77(2)
Mg3-O2b	2.07(1)	Mg4-O10	2.18(3)
Mg3-O3b	2.04(1)	Mg4-O3b	2.07(1)
Mg3-O4b	2.05(1)	Mg4-O4b	2.06(1)
<Mg3-O>	2.06	<Mg4-O>	2.20
O10-O3	2.87(3)	O10-O4	2.90(3)
O10-O8	2.89(4)	O10-O4b	2.96(3)

Note: Soft constraints were applied to Si-O and Mg-O distances (except Mg4-O10) during refinements.

RESULTS AND DISCUSSION

Sepiolite at RT in air

In general, the refined sepiolite model determined using the XRD data collected at room temperature in air (Fig. 1) compares well with that deduced by Brauner and Preisinger (1956). In addition to minor differences in some of the atom positions, the refinement revealed an additional zeolitic H_2O site.

The refined Mg-O distances range from 2.04 to 2.12 Å (Table 5), consistent with relatively undistorted Mg-O octahedra. The mean Mg-O distances for the four unique octahedra (2.06–2.09 Å) are close to the ideal value of 2.08 Å (Shannon 1976), which is consistent with the microprobe analyses indicating that only Mg resides in the octahedral sites. As discussed above, the Si-O distances were softly constrained during the refinement, and all fall in the range of 1.60–1.64 Å (Table 5).

The sepiolite model of Brauner and Preisinger (1956) contains three hydrous species: OH^- anions at the O2 site, coordinated to Mg1, Mg 2, and Mg3; structural H_2O at the O10 site, where it completes the Mg4 coordination at the edges of the Mg-(O, OH, H_2O) octahedral strips; and three zeolitic H_2O positions in the tunnels. Because of the negligibly small X-ray scattering factor for H, we were unable to locate the positions of the H atoms, and we assumed that O2 is OH^- and O10 is structural H_2O. The refined occupancy factor for the O10 site indicated that it is fully occupied. No evidence was found for split Mg4 and O10 sites as reported by Rautureau and Tchoubar (1976) from their electron diffraction study. These authors suggested that these split sites might be a feature of sepiolite in vacuum, as was the case for their sample in the TEM. However, no evidence was observed that Mg4 and O10 occupy split sites in the structure even for data collected from a sepiolite sample under vacuum.

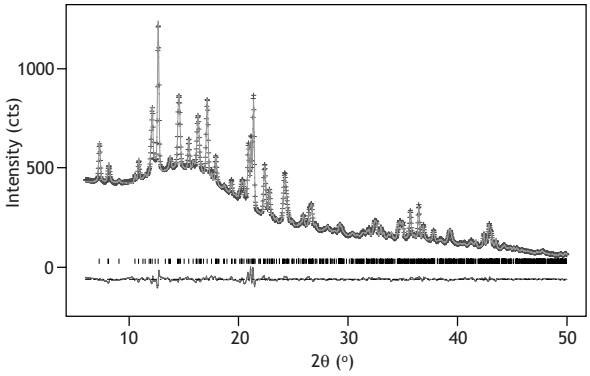

FIGURE 3. Final observed (crosses), calculated (solid line), and difference (lower) patterns for the Rietveld refinement for sepiolite in air using the RT synchrotron powder X-ray diffraction data.

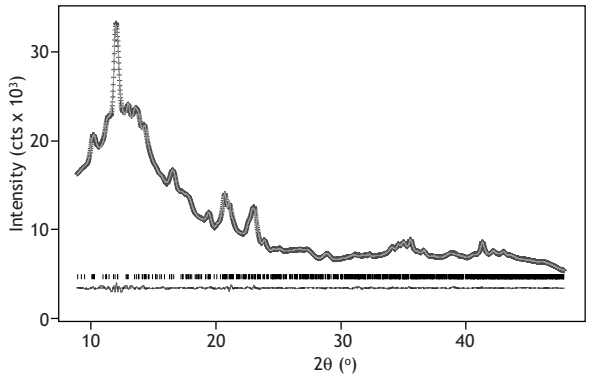

FIGURE 4. Final observed (crosses), calculated (solid line), and difference (lower) patterns for the Rietveld refinement for sepiol-2H_2O in air using synchrotron powder X-ray diffraction data collected at ~742 K.

Difference-Fourier maps and subsequent Rietveld refinement revealed four zeolitic H_2O sites, three of which (O11, O12, and O13) are close to those in the Brauner and Preisinger (1956) model. Refined occupancy factors indicated that the O11 and O12 sites are at full occupancy, or nearly so, O13 is approximately one-half filled, and O14 (not reported by Brauner and Preisinger 1956) is about one-third occupied. The total of ~15.6 zeolitic H_2O molecules per unit cell determined by refinement is in reasonable agreement (within errors of the occupancy factors) with the value of ~16 reported in the chemical formula determined by Preisinger (1959) from wet chemical analyses. The interatomic distances among the zeolitic H_2O (O) sites range from 2.32 to 3.01 Å (Table 5) and considering the errors are typical for H-bonded distances.

The O14-O14 distance of 1.64 Å indicates that H_2O molecules cannot occupy adjacent O14 sites and this is consistent with a refined occupancy for the site of less than one-half. The O12 and O14 sites are the only zeolitic H_2O molecules within reasonable H-bonded distances, 2.72 and 2.47 Å, respectively, of the O10 (structural H_2O); O14 is 2.64 Å from O8 and is the only zeolitic H_2O molecule close to one of the framework O atoms. These results are similar to those of Giustetto and Chiari (2004) who recently reported a neutron diffraction study of palygorskite, which has a slightly smaller tunnel structure than that of sepiolite. They determined that the structural H_2O in palygorskite that is comparable to O10 in sepiolite also forms apparent H-bonds with two of the zeolitic H_2O molecules, at distances of ~2.55 and 2.85 Å. Thus, although the zeolitic H_2O molecules in sepiolite exhibit a reasonable degree of H-bonding among themselves, they are not strongly linked to the surrounding structural framework, perhaps explaining why they are easily lost when sepiolite is exposed to vacuum or undergoes gentle heating.

Sepiolite in vacuum

The refined atomic coordinates for the sepiolite framework under vacuum are not significantly different from those in air. The major difference between the two structures is loss of most of the zeolitic H_2O from the sepiolite in vacuum (Fig. 1), and the consequent adjustment of the unit-cell parameters (Table 1). Difference-Fourier maps for the evacuated material show only a single electron-density peak in the tunnels (O11 in Table 3), near the O14 position of sepiolite in air (Table 3), and the refinement of the occupancy factor indicates that the site is approximately one-quarter filled (~2 H_2O/cell). Therefore, sepiolite under vacuum, even at room temperature, releases ~7/8 of its zeolitic H_2O. The three unit-cell edges decrease slightly with the H_2O loss, the major change occurring along *a* (decrease of ~1.2%, vs. an increase of 0.1% for *b* and decrease of 0.2% for *c* (Table 1), resulting in a volume decrease of ~1.3%. Thus, the loss of the zeolitic H_2O induces the sepiolite tunnels to collapse slightly along *a* and to relax along *b*.

In-situ heating experiment

The synchrotron X-ray diffraction data (Fig. 5) reveal an obvious phase change at ~600–650 K for sepiolite heated in air, and this transition presumably corresponds to the folding of the sepiolite structure as the first half of the structural H_2O (O10) is lost (Preisinger 1959, 1963; Nagata et al. 1974). This sepiolite "anhydride" was designated as "sepiol-2H_2O," following the nomenclature of Kitayama et al. (1999), where "2H_2O" refers to the two remaining structural H_2O molecules, from the original four (based on a chemical formula normalized to 8 Mg atoms). Preisinger (1963) was the first to describe this dehydration product when sepiolite is heated above ~650 K, and he reported the phase as monoclinic ($P2_1/n$).

RT to 600 K. During the temperature-resolved synchrotron XRD heating of sepiolite in air, the unit-cell volume decreased continuously by ~0.7% between 300 and 390 K accompanied by a decrease in *a* and *c* and a slight increase in *b* (Fig. 6). Rietveld refinements using the XRD data indicated that most of the zeolitic H_2O is lost over this same temperature range (Fig. 7). Similarly, Kitayama et al. (1999) observed a loss of zeolitic H_2O from sepiolite near 373 K, and TGA measurements of sepiolite by Nagata et al. (1974) indicated that H_2O is lost continuously from just above RT to ~383 K. Serna et al. (1975) observed H_2O loss in air from RT to ~450 K with a DTG peak at 383 K.

The Rietveld refinements indicated that as sepiolite is heated, H_2O is lost at approximately the same rate from all of the zeo-

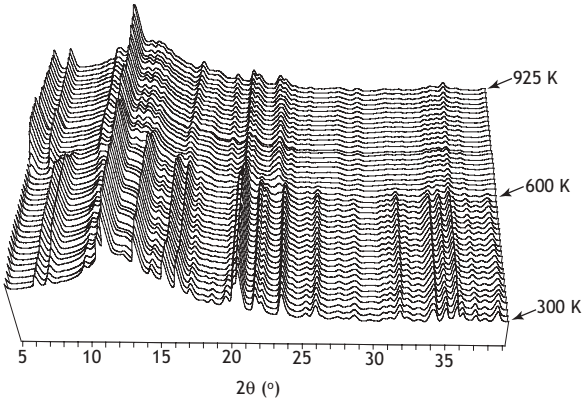

FIGURE 5. Synchrotron powder X-ray diffraction patterns for sepiolite in air vs. temperature, from 300 K (front pattern) to 925 K. The transformation to the folded sepiol-2H_2O phase occurs in the range 600 to 650 K.

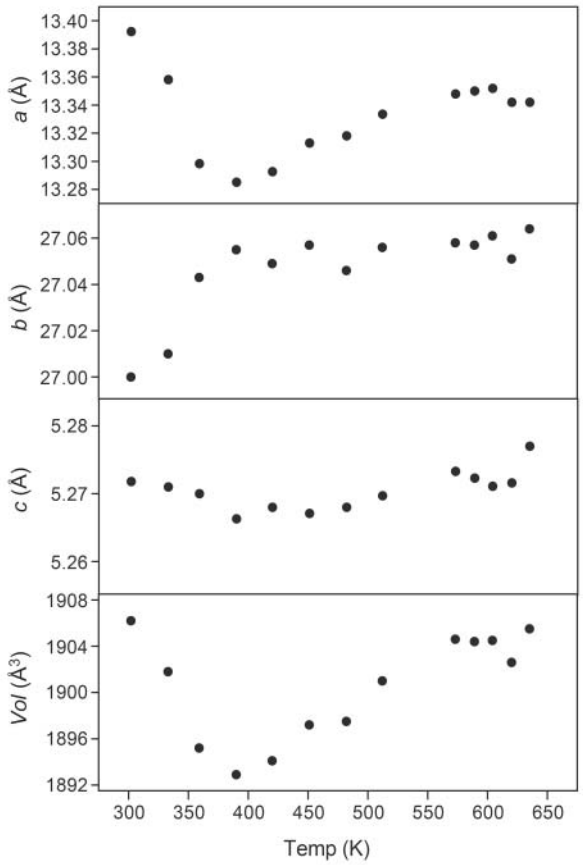

FIGURE 6. Plots of sepiolite unit-cell parameters vs. *T* for the range 300 to 600 K. The errors determined by the refinements are within the plotting symbols.

litic H_2O sites. The occupancy refinements suggested that small amounts of H_2O remain on the O14 and O11 sites to near 473 K. Note, however, that these small residual occupancies are near zero, within error; they might be artifacts resulting from correlations during the least-squares refinements among the occupancy factors, background coefficients and displacement parameters. In contrast, TGA studies (e.g., Serna et al. 1975) showed that zeolitic H_2O loss might continue to at least ~450 K. Also, as discussed above, O14 probably forms H-bonds with O10 and O8, and therefore, some H_2O molecules might linger at this site to higher temperatures. Above 390 K, there is a continual thermal expansion of the sepiolite structure to ~573 K (Fig. 6). The unit-cell volume increases by 0.6%, with most of the change occurring in *a* (+0.5%), probably corresponding to a slight inflation of the tunnel in that direction. Previous studies show that for sepiolite samples heated to less than ~625 K, zeolitic H_2O is quickly replaced at ambient temperature and humidity (e.g., Preisinger 1959).

600 to 925 K. The powder XRD patterns in Figure 5 show the first appearance of sepiol-2H_2O at ~600 K, as indicated by diffraction peaks at ~10.3 and 8.2 Å (~5° and 6° 2θ, respectively in Fig. 5), and over the next ~50 K the diffraction intensity for sepiol-2H_2O increases as the sepiolite peaks diminish, until at ~650 K only sepiol-2H_2O remains. Rietveld refinements of the sepiolite structure using diffraction patterns in this temperature range did not indicate any decrease in the O10 (structural H_2O) occupancy prior to the phase change. This result suggests that the initial loss of O10 and consequent folding of the structure occur quickly, and the refined model reflects only the diminishing fraction of the sepiolite sample that retains all of its O10. This rapid transition is consistent with dehydration studies of Nagata et al. (1974) and Serna et al. (1975) that show narrow, intense DTA peaks associated with the first loss of structural H_2O centered at ~573 and ~603 K, respectively. Serna et al. (1975) noted that the temperature range of the phase transition is dependent on the experimental conditions, such as the heating rate or whether the sample was heated in air or vacuum. Nonetheless, the transition temperature range observed in this study is consistent with those reported by previous researchers.

The refined model for sepiol-2H_2O confirms that proposed by Preisinger (1959, 1963). The loss of one-half of the structural H_2O causes the sepiolite phyllosilicate ribbons to rotate, or fold, thereby reducing the cross-sectional area of the tunnels and lowering the structure symmetry from orthorhombic to monoclinic. The unit-cell parameters for sepiol-2H_2O at 742 K are listed in Table 2 and differ slightly from those proposed by Preisinger (1963); the *b* parameter is larger (11.35 Å rather than 10.9 Å), and β is ~89° instead of 90°.

The loss of one-half of the O10 H_2O molecules requires Mg4 to complete its octahedral coordination in sepiol-2H_2O by forming a bond, albeit a long one (2.76 Å), to one of the tetrahedral O atoms (O8) (Fig. 2). The Si-O bond constraints used during the refinements, however, might prevent complete refinement that could result in a shorter Mg4-O8 distance. The need to complete the Mg4 coordination octahedron after the loss of one of the O10 H_2O molecules might be the major driving force to cause the sepiolite structure to fold, facilitated by having fewer O10 H_2O molecules to prop open the tunnels.

Difference-Fourier maps calculated using only the sepiol-2H_2O framework atoms revealed the position of the remaining O10 H_2O molecule in the tunnel. The refined occupancy factor for O10 did not differ significantly from 1.0 for temperatures less than ~820 K. Above this temperature, the occupancy factor declined steadily (Fig. 8) to ~0.5 at 925 K, presumably as sepiol-2H_2O transformed to "anhydrous" sepiolite (though the hydroxyl was retained in this high-temperature structure). Refinement using a second data set collected after heating at 925 K for an additional 12 minutes yielded an O10 occupancy factor of 0.4, suggesting that the heating rate was not yielding equilibrium loss of O10. In fact, DTA measurements by Nagata et al. (1974) show a considerably broader peak associated with the loss of the residual O10, compared with that for the initial O10, indicating a more gradual loss over a larger temperature range (673 to 893 K). Serna et al. (1975) argue that it is more difficult for the second half of the O10 water molecules to leave the structure because they are entrapped within the collapsed tunnels.

Lokanatha et al. (1985) described the loss of the second bound H_2O molecule between 723 and 873 K, and their XRD radial distribution study revealed a decrease in the Mg4 coordination between 673 and 873 K. Bond distances calculated from our refined models indicated a lengthening of the Mg4-O10 distance from ~2.13 to 2.32 Å over the temperature range ~790 to 900 K. With the loss of all O10 H_2O, Mg4 is coordinated to four O atoms at ~2.06 Å and O8 at 2.67 Å. Our diffraction studies and previous experiments (Lokanatha et al. 1985) show that as hydroxyl

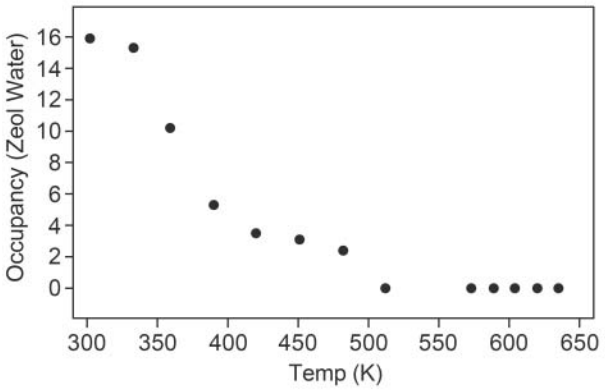

FIGURE 7. Plot of total number of zeolitic H_2O molecules determined by Rietveld refinements vs. *T*.

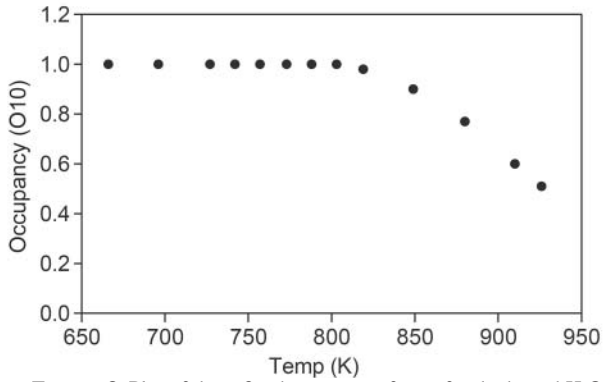

FIGURE 8. Plot of the refined occupancy factor for the bound H_2O (O10) in sepiol-2H_2O vs. *T*.

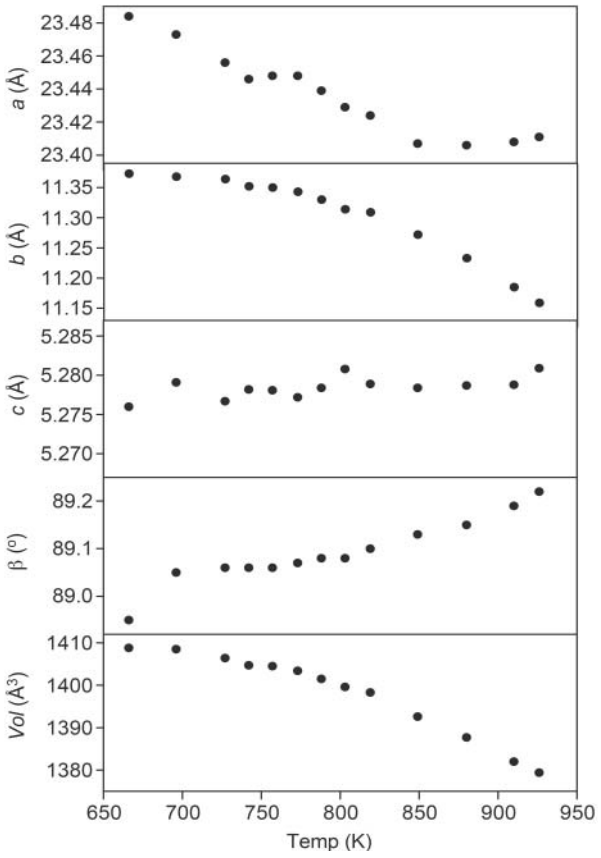

FIGURE 9. Plots of sepiol-2H_2O and "anhydrous" sepiolite (>~820 K) unit-cell parameters vs. *T* for the range 600 to 925 K. The errors determined by the refinements are within the plotting symbols.

groups are lost above ~1050 K an amorphous phase results.

The unit-cell parameters for the folded sepiolite structure are plotted as a function of temperature in Figure 9. In general, *a*, *b*, and volume steadily decrease with increasing temperature and β approaches 90°; there is an obvious change in slope at ~820 K suggesting a phase transformation. The fact that the O10 occupancy factor also begins to decrease at about the same temperature (Fig. 8) strongly indicates that the phase change is caused by the loss of the second half of the bound H_2O molecules (O10), i.e., sepiol-2H_2O changes to "anhydrous" sepiolite (with OH). Nagata et al. (1974) similarly noted a discontinuous change in powder XRD peaks for samples heated between 623 and 723 K and suggested that there were two distinct dehydrated phases, one at 573 and another at 873 K. In contrast, Serna et al. (1975) did not observe any structural changes with the loss of the second bound H_2O. Our results clearly suggest the existence of two distinct phases, one containing one-half of the bound H_2O molecules and the other with no bound H_2O. Above 820 K, *b*, β, and volume continue to decrease, but *a* is unchanged.

ACKNOWLEDGMENTS

This work was supported by National Science Foundation grant no. EAR04-17714. The TGA data were collected by Blythe McCarthy. We received invaluable assistance from Jonathan Hanson at the National Synchrotron Light Source, X-7B. The manuscript was greatly improved by reviewers Roberto Giustetto, Mark Krekeler, and Richard Thompson and by skillful and perceptive handling by Associate Editor Stephen Guggenheim.

REFERENCES CITED

Brauner, K. and Preisinger, A. (1956) Struktur und Entstehung des Sepioliths. Tschermaks Mineralogische und Petrographische Mitteilungen, 6, 120–140.

Brown, G.E., Sueno, S., and Prewitt, C.T. (1973) A new single-crystal heater for the precession camera and four-circle diffractometer. American Mineralogist, 58, 698–704.

Cámara, F., Garvie, L.A.J., Devouard, B., Groy, T.L., and Buseck, P.R. (2002) The structure of Mn-rich tuperssuatsiaite: a palygorskite-related mineral. American Mineralogist, 87, 1458–1463.

Finger, L.W., Cox, D.E., and Jephcoat, A.P. (1994) A correction for powder diffraction peak asymmetry due to axial divergence. Journal of Applied Crystallography, 27, 892–900.

Giustetto, R. and Chiari, G. (2004) Crystal structure refinement of palygorskite from neutron powder diffraction. European Journal of Mineralogy, 16, 521–532.

Hammersley, A.P., Svensson, S.O., Hanfland, M., Fitch, A.N., and Hausermann, D. (1996) Two-dimensional detector software: From real detector to idealised image or two-theta scan. High Pressure Research, 14, 235–248.

Hayashi, H. (1969) Infrared study of sepiolite and palygorskite on heating. American Mineralogist, 53, 1613–1624.

Jones, B.F. and Galan, E. (1988) Sepiolite and palygorskite. In S.W. Bailey, Ed., Hydrous Phyllosilicates, 19, p. 631–674. Reviews in Mineralogy, Mineralogical Society of America, Chantilly, Virginia.

Kitayama, Y., Kamimura, M., Wakui, K., Kanamori, M., Kodama, T., and Abe, J. (1999) Cyclodehydration of diethylene glycol (DEG) catalyzed by clay mineral sepiolite. Journal of Molecular Catalysis A: Chemical, 142, 237–245.

Larson, A.C. and Von Dreele, R.B. (2001) GSAS-General Structure Analysis System. Los Alamos National Laboratory Report No. LAUR 86-748.

Lokanatha, S., Mathur, B.K., Samantaray, B.K., and Bhattacherjee, S. (1985) Dehydration and phase transformation in sepiolite—a radial distribution analysis study. Zeitschrift für Kristallographie, 171, 69–79.

Nagata, H., Shimoda, S., and Sudo, T. (1974) On dehydration of bound water of sepiolite. Clays and Clay Minerals, 22, 285–293.

Pluth, J., Smith, J., Pushcharovskii, D.Y., Semenov, E.I., Bram, A., Riekel, C., Weber, H., and Broach, R.W. (1997) Third-generation synchrotron X-ray diffraction of 6-μm crystal of raite, ≈$Na_3Mn_3Ti_{0.25}Si_8O_{20}(OH)_2 \cdot 10H_2O$, opens up new chemistry and physics of low-temperature minerals. Proceedings of the National Academy of Sciences U.S.A., 94, 12263–12267.

Post, J.E. and Bish, D.L. (1989) Rietveld refinement of crystal structures using powder X-ray diffraction data. In D.L. Bish and J.E. Post, Eds., Modern Powder Diffraction, 20, p. 277–308. Reviews in Mineralogy, Mineralogical Society of America, Chantilly, Virginia.

Preisinger, A. (1959) X-ray study of the structure of sepiolite. Clays and Clay Minerals, 6, 61–67.

——— (1963) Sepiolite and related compounds: its stability and application. Clays and Clay Minerals, 10, 365–371.

Rautureau, M. and Mifsud, A. (1977) Etude par microscope electronique des differents etats d'hydration de la sepiolite. Clay Minerals, 12, 309–318.

Rautureau, M. and Tchoubar, C. (1976) Structural analysis of sepiolite by selected area electron diffraction—relations with physico-chemical properties. Clays and Clay Minerals, 24, 43–49.

Ruiz, R., del Moral, J.C., Pesquera, C., Benito, I., and González, F. (1996) Reversible folding in sepiolite: study by thermal and textural analysis. Thermochimica Acta, 279, 103–110.

Ruiz-Hitzky, E. (2001) Molecular access to intracrystalline tunnels of sepiolite. Journal of Materials Chemistry, 11, 86–91.

Serna, C., Ahlrichs, J.L., and Serratosa, J.M. (1975) Folding in sepiolite crystals. Clays and Clay Minerals, 23, 452–457.

Shannon, R.D. (1976) Revised effective ionic radii and systematic studies of interatomic distances in halides and chalcogenides. Acta Crystallographica, A32, 751–767.

Stephens, P.W. (1999) Phenomenological model of anisotropic peak broadening in powder diffraction. Journal of Applied Crystallography, 32, 281–289.

Thompson, P., Cox, D.E., and Hastings, J.B. (1987) Rietveld refinement of Debye-Scherrer synchrotron X-ray data from Al_2O_3. Journal of Applied Crystallography, 20, 79–83.

Van Scoyoc, G.E., Serna, C., and Ahlrichs, J.L. (1979) Structural changes in palygorskite during dehydration and dehydroxylation. American Mineralogist, 64, 216–223.

Wang, Q.K., Matsuura, T., Feng, C.Y., Weir, M.R., Detellier, C., Rutadinka, R.L., and Van Mao, R.L. (2001) The sepiolite membrane for ultrafiltration. Journal of Membrane Science, 184, 153–163.

Weir, M.R., Kuang, W., Facey, G.A., and Detellier, C. (2002) Solid-state nuclear magnetic resonance study of sepiolite and partially dehydrated sepiolite. Clays and Clay Minerals, 50, 240–247.

MANUSCRIPT RECEIVED NOVEMBER 1, 2005
MANUSCRIPT ACCEPTED JULY 19, 2006
MANUSCRIPT HANDLED BY STEPHEN GUGGENHEIM